

MULTICORE-OPTIMIZED WAVEFRONT DIAMOND BLOCKING FOR OPTIMIZING STENCIL UPDATES

T. MALAS¹, G. HAGER², H. LTAIEF¹, H. STENGEL², G. WELLEIN², AND D. KEYES¹

Abstract. The importance of stencil-based algorithms in computational science has focused attention on optimized parallel implementations for multilevel cache-based processors. Temporal blocking schemes leverage the large bandwidth and low latency of caches to accelerate stencil updates and approach theoretical peak performance. A key ingredient is the reduction of data traffic across slow data paths, especially the main memory interface. In this work we combine the ideas of multicore wavefront temporal blocking and diamond tiling to arrive at stencil update schemes that show large reductions in memory pressure compared to existing approaches. The resulting schemes show performance advantages in bandwidth-starved situations, which are exacerbated by the high bytes per lattice update case of variable coefficients. Our thread groups concept provides a controllable trade-off between concurrency and memory usage, shifting the pressure between the memory interface and the CPU. We present performance results on a contemporary Intel processor.

1. Introduction.

1.1. Stencil codes. The evaluation of stencil operators on Cartesian lattices is a classic kernel in computational science and engineering, arising from systems that are born discrete and from discretizations of PDEs, both explicit and implicit. In the implicit case the iteration index is analogous to explicit time and stencil evaluation becomes a case of sparse matrix-vector multiplication with special structure. Lattice values are updated from neighbors at a previous level with concurrency that scales linearly with the number of degrees of freedom. However, low flop-per-byte ratios put a premium on locality. Regular access patterns allow high spatial locality, in the sense of packing cache blocks. The modest temporal locality within a single iteration level from reuse of a value within several adjacent stencils can be enhanced across iteration levels.

A major demarcation exists between stencils whose coefficients are constant in space and time and those that vary, since variable coefficients can shift the dominant workingset from the lattice values being updated to the coefficients, themselves. In the PDE context, coefficient variability can arise from constitutive parameters (conductivities, elastic moduli, etc.) that depend upon space or time intrinsically or through dependences on the evolving field values, themselves, the typical nonlinear case. Some models can be scaled so that the variability affects only the diagonal term of the stencil, which is then an important case to which to specialize. Whether to compute coefficients on-the-fly is a decision that affects the hardware resource balance, since it both releases all of the memory bandwidth to the lattice values and increases the flop intensity of the typical lattice update.

Locality is also affected in a major way by the truncation order of the discretization, which manifests itself in the stencil size, each lattice value appearing in more stencil evaluations. Trends in PDE modeling towards high-order discretizations and high fidelity physics shift interest beyond the low-order constant-coefficient models to which most computer science optimizations have been directed to date. For instance, seismic models used in oil exploration are typically eighth-order and variable coefficients are the norm. Traditional means of obtaining high truncation order by

¹Extreme Computing Research Center (ECRC), King Abdullah University of Science and Technology (KAUST), Saudi Arabia

²Erlangen Regional Computing Center (RRZE), Friedrich-Alexander University of Erlangen-Nuremberg, Germany

expanding the spatial extent of the stencil to distributed memory parallelization of stencil evaluation by expanding the halo region. More spatially compact means of obtaining high order are therefore of interest.

The aforementioned issues put once-humble stencil evaluation in the cross-hairs of co-design and motivate our examination of several shared-memory (multi-core) and distributed-memory (message-passing) optimizations of a variety of stencils (see Figure 3.1) on state-of-the-art hardware. We are especially concerned with the degradation of memory bandwidth per core forecast at tomorrow’s extreme scale. We combine classical and novel techniques and test them on a range of star-like stencils accommodating up to eighth-order, constant and variable coefficient (without on-the-fly recomputation), noting their salutary effects on memory pressure, power consumption, and obtainable performance, and noting the transition of hardware bottlenecks.

This paper merely scratches the surface of co-design for the fundamental kernel of Cartesian lattice updates. Pipelined or s-step Krylov solvers, time-parallelism, and high-order temporal discretizations that are obtained by using the governing PDE to estimate high time derivatives with high space derivatives are all potentially stencil-expanding (and halo-expanding) decisions made at an upstream algorithmic stage. Their downstream consequences on stencil update performance and hardware balance can be examined using the analyses and software tools introduced herein, but it remains to close the loop with analyses and tools that allow how to design the best discrete schemes in the first place.

1.2. Contribution. This work makes the following contributions: We combine two previously known concepts for optimizing stencil computations, diamond tiling and multi-core aware temporal wavefront blocking, and show our method to be more efficient in terms of flexibility, cache requirements, and main memory pressure than either concept by itself on a modern Intel 10-core CPU. Our method shows best performance for stencil types with low computational intensity, such as long-range stencils with variable coefficients. The reduced memory bandwidth pressure has a positive side effect of significant energy savings in memory. We also show that MPI parallelization of the method is straightforward and enables natural overlapping of computation and communication.

The rest of this paper is organized as follows: After an overview of related work in Sect. 2 we introduce the test system, define some basic terminology, and study a variety of stencil update schemes together with baseline performance data without temporal blocking but otherwise minimal code balance in Sect. 3. In Sect. 4 we briefly review multi-core wavefront temporal blocking and diamond tiling before elaborating on the combination of the two concepts in Section 5. In Sect. 6 we present performance results, and Sect. 7 provides a summary and an outlook to possible future work.

2. Related work. The importance of stencil computations and the inefficient performance of their naïve implementations on modern processors motivates researchers to study them extensively. The optimizations required to achieve the desired performance depend on the properties of the stencil operator and the capabilities of different resources in the processor. This case is made by Datta [5], where the performance of several combinations of optimization techniques, processors, and stencil operators is reported.

The high bytes per lattice site update (LUP) requirement of many stencil computations and the increasing performance gap between the arithmetic operations and the data transfer are the major concerns in achieving high performance. Spatial and

temporal blocking improve the performance by increasing the data reuse in the cache memory of modern processors.

Spatial blocking is an established technique that changes the grid traversal order to maximise the data reuse in the desired memory level [6, 7]. Temporal blocking allows more data reuse in the cache memory by reordering grid traversal across space iterations, where blocks of grid points are accessed multiple times before completing the traversal of a single spatial grid level.

Temporal blocking techniques require careful handling of data dependencies across space iterations to ensure correctness. Several tiling techniques are proposed in the literature including: parallelepiped, split, overlapped, diamond, and hexagonal. These block shapes optimize for data locality, concurrency, or both. Reviews of these techniques can be found at Orozco *et al.* [22] and Zhou [33]. We believe that diamond tiling is promising for efficiently providing both concurrency and data locality over the problems and computer architectures of our interest. Its attractiveness in recent years is evident in: [22], [33], Strzodka *et al.* [26], Bandishti *et al.* [1], and Grosser *et al.* [10], where a GPU implementation of hexagonal tiling is proposed, then a study of hexagonal and diamond tiling is performed [11].

The wavefront technique, which is introduced by Lamport [15] (using the name “hyperplane”), performs temporal blocking at adjacent grid points. This technique has been combined with other tiling approaches using single-thread wavefront temporal blocking as in [26], Wonnacott *et al.* [31], and Nguyen *et al.* [20], and using multi-threaded wavefront temporal blocking, as in Wellein *et al.* [29].

Cache optimization techniques can be classified into cache-oblivious and cache-aware techniques. Cache-oblivious techniques [8, 27, 25] do not need prior knowledge or tuning to find optimal cache block size to achieve high performance stencil computations. On the other hand, cache-aware techniques utilize auto-tuning as in [5], which performs parameter search over the optimization techniques to achieve best performance. Another cache-aware algorithm is introduced in [26], where cache block size calculations are used to set the cache block size that achieves best performance.

Several frameworks have been developed to produce optimized stencil codes. PLUTO [2] is a source-to-source transformation tool that uses polyhedral model, CATS [26] is a library, Pochoir [27] uses cache-oblivious algorithms in Domain Specific Languages (DSL), PATUS [4] uses auto-tuning with a DSL, and Henretty *et al.* [14] develop a DSL that uses split-tiling. Unat *et al.* [28] introduced Mint, a programming model that produces highly optimized GPU code from a user’s annotated traditional C code. Physis, a DSL that generates optimized GPU codes with the necessary MPI calls for heterogeneous GPU clusters, was proposed by Maruyama *et al.* [17]. A recent review paper of stencil optimization tools that use polyhedral model has been prepared by Wonnacott [32].

3. Detailed analysis of various stencil operators.

3.1. Definitions and terminology. In iterative stencil computations, each point in a multi-dimensional spatial grid (Ω) is updated using weighted contributions from its neighbor points, defined by the stencil operator. The stencil operator specifies the relative coordinates of the contributing points and their weights. The weights can be constant or variable in space and/or time with some or no symmetry to be exploited around the updated point. The grid update operation over the complete spatial domain (one “sweep”) is repeated T times (time steps or iterations). We consider three-dimensional grids in this work ($\Omega := \{1, \dots, N_x\} \times \{1, \dots, N_y\} \times \{1, \dots, N_z\}$), where x is the leading dimension, followed by the y and z dimensions. A grid location

(x_1, y_1, z_1) at time step τ can be expressed as Ω_{z_1, y_1, x_1}^t . We also follow the common practice regarding the mapping of the spatial and temporal domain to a data structure in the C language: $\Omega_{z, y, x}^t$ is stored as $\Omega[\tau][z][y][x]$, where the spatial indices x , y , and z can assume integer values in the range $0 \dots N_i - 1$ so that the innermost loop accesses memory with a stride of one. The time index can only assume the values 0 and 1, so the data from time step $t - 1$ is overwritten by the new data for $t + 1$ in each grid update. PDE discretizations higher than first order in temporal truncation error can often be accommodated by employing the original underlying PDE to replace higher-order-in-time derivatives in the truncation error with their spatial equivalent. This expands the spatial stencil while keeping the number of domain copies at minimum. Figure 3.1 shows several examples of stencil computation kernels that use a “Jacobi-like” update scheme where the stencil array (i.e., the data structure with read access to neighboring grid points) is not written to during the same sweep. Another possible variant is “Gauss-Seidel” update scheme, where the stencil array is adapted during the same sweep. The latter is relevant in practice but beyond the scope of this paper. All stencils considered here are “star stencils” of various spatial differential or truncation orders. “Box stencils”, “diamond stencils”, and multicomponent stencils, in which multiple discrete fields interact on the same (or interlaced, staggered) lattices, are also important in practice, and can be handled with similar techniques.

3.2. Test systems. All benchmark tests were performed on a cluster of dual-socket Intel Ivy Bridge (Xeon E5-2660v2) nodes with a nominal clock speed of 2.2 GHz and ten cores per chip. The “Turbo Mode” feature was disabled. Each CPU has a 25 MiB L3 cache which is shared among all cores, and core-private L2 and L1 caches of 256 KiB and 32 KiB, respectively. All data paths between the cache levels are half-duplex, 256-bit wide buses, so the transfer of one 64-byte cache line between adjacent caches takes two CPU cycles. The core architecture supports all Intel Single Instruction Multiple Data (SIMD) instruction sets up to AVX (Advanced Vector Extensions). With AVX, one core is able to sustain one full-width (32 byte) load and one half-width (16 byte) store per cycle. In addition, one AVX multiply and one AVX add instruction can be executed per cycle. Since one AVX register can hold either four double precision (DP) or eight single precision (SP) operands, the peak performance of one core is eight flops per cycle in DP or sixteen flops per cycle in SP.

Each node is equipped with 64 GB of DDR3-1600 RAM per socket and has a maximum attainable memory bandwidth of $b_S \approx 40$ GB/s per socket (as measured with the STREAM COPY [18] [19] benchmark). The nodes are connected by a full non-blocking, fat-tree QDR InfiniBand network.

For compiling and linking, the Intel C compiler in version 13.1.3 was used together with the Intel MPI library 4.1.3. Hardware performance counter measurements were done with `likwid-perfctr` from the LIKWID multicore tools collection [16].

3.3. Performance prediction and measurements for pure spatial blocking. In this section we analyze two basic stencil update schemes for their requirements on the hardware. It is not our goal to provide a comprehensive coverage of all possible variations in stencil algorithms; we rather wish to motivate that our selection includes relevant corner cases. We use (LUP/s) as a basic performance metric, since it does not contain any uncertainty as to how many flops are actually done during one stencil update. Specific implementations have a fixed ratio of LUPs to flops and other relevant hardware events (such as bytes transferred, instructions executed, etc.), which are discussed as required. Unless otherwise noted, the working set does not fit into any CPU cache.

$$\begin{aligned}
& \text{for } t = 0 \text{ to } T - 1 \\
& \quad \text{for } x = 1 \text{ to } N_x \\
& \quad \quad \Omega_x^{t+1} = w_1 * \Omega_x^t \\
& \quad \quad \quad + w_2 * (\Omega_{x-1}^t + \Omega_{x+1}^t)
\end{aligned}$$

(a) 1st order in time 3-point constant-coefficient stencil in one dimension, with symmetry.

$$\begin{aligned}
& \text{for } t = 0 \text{ to } T - 1 \\
& \quad \text{for } z = 1 \text{ to } N_z \\
& \quad \quad \text{for } y = 1 \text{ to } N_y \\
& \quad \quad \quad \text{for } x = 1 \text{ to } N_x \\
& \quad \quad \quad \quad \Omega_{z,y,x}^{t+1} = w_1 * \Omega_{z,y,x}^t \\
& \quad \quad \quad \quad \quad + w_2 * (\Omega_{z,y,x-1}^t + \Omega_{z,y,x+1}^t) \\
& \quad \quad \quad \quad \quad + w_2 * (\Omega_{z,y-1,x}^t + \Omega_{z,y+1,x}^t) \\
& \quad \quad \quad \quad \quad + w_2 * (\Omega_{z-1,y,x}^t + \Omega_{z+1,y,x}^t)
\end{aligned}$$

(b) 1st order in time 7-point constant-coefficient isotropic stencil in three dimensions, with symmetry.

$$\begin{aligned}
& \text{for } t = 0 \text{ to } T - 1 \\
& \quad \text{for } z = 1 \text{ to } N_z \\
& \quad \quad \text{for } y = 1 \text{ to } N_y \\
& \quad \quad \quad \text{for } x = 1 \text{ to } N_x \\
& \quad \quad \quad \quad \Omega_{z,y,x}^{t+1} = \\
& \quad \quad \quad \quad \quad W_{0,z,y,x} * \Omega_{z,y,x}^t \\
& \quad \quad \quad \quad \quad + W_{1,z,y,x} * \Omega_{z,y,x-1}^t \\
& \quad \quad \quad \quad \quad + W_{2,z,y,x} * \Omega_{z,y,x+1}^t \\
& \quad \quad \quad \quad \quad + W_{3,z,y,x} * \Omega_{z,y-1,x}^t \\
& \quad \quad \quad \quad \quad + W_{4,z,y,x} * \Omega_{z,y+1,x}^t \\
& \quad \quad \quad \quad \quad + W_{5,z,y,x} * \Omega_{z-1,y,x}^t \\
& \quad \quad \quad \quad \quad + W_{6,z,y,x} * \Omega_{z+1,y,x}^t
\end{aligned}$$

(c) 1st order in time 7-point variable-coefficient stencil in three dimension, with no coefficient symmetry.

$$\begin{aligned}
& \text{for } t = 0 \text{ to } T - 1 \\
& \quad \text{for } z = 1 \text{ to } N_z \\
& \quad \quad \text{for } y = 1 \text{ to } N_y \\
& \quad \quad \quad \text{for } x = 1 \text{ to } N_x \\
& \quad \quad \quad \quad \Omega_{z,y,x}^{t+1} = W_{0,z,y,x} * \Omega_{z,y,x}^t \\
& \quad \quad \quad \quad \quad + W_{1,z,y,x} * (\Omega_{z,y,x-1}^t + \Omega_{z,y,x+1}^t) \\
& \quad \quad \quad \quad \quad + W_{2,z,y,x} * (\Omega_{z,y-1,x}^t + \Omega_{z,y+1,x}^t) \\
& \quad \quad \quad \quad \quad + W_{3,z,y,x} * (\Omega_{z-1,y,x}^t + \Omega_{z+1,y,x}^t) \\
& \quad \quad \quad \quad \quad + W_{4,z,y,x} * (\Omega_{z,y,x-2}^t + \Omega_{z,y,x+2}^t) \\
& \quad \quad \quad \quad \quad + W_{5,z,y,x} * (\Omega_{z,y-2,x}^t + \Omega_{z,y+2,x}^t) \\
& \quad \quad \quad \quad \quad + W_{6,z,y,x} * (\Omega_{z-2,y,x}^t + \Omega_{z+2,y,x}^t) \\
& \quad \quad \quad \quad \quad + W_{7,z,y,x} * (\Omega_{z,y,x-3}^t + \Omega_{z,y,x+3}^t) \\
& \quad \quad \quad \quad \quad + W_{8,z,y,x} * (\Omega_{z,y-3,x}^t + \Omega_{z,y+3,x}^t) \\
& \quad \quad \quad \quad \quad + W_{9,z,y,x} * (\Omega_{z-3,y,x}^t + \Omega_{z+3,y,x}^t) \\
& \quad \quad \quad \quad \quad + W_{10,z,y,x} * (\Omega_{z,y,x-4}^t + \Omega_{z,y,x+4}^t) \\
& \quad \quad \quad \quad \quad + W_{11,z,y,x} * (\Omega_{z,y-4,x}^t + \Omega_{z,y+4,x}^t) \\
& \quad \quad \quad \quad \quad + W_{12,z,y,x} * (\Omega_{z-4,y,x}^t + \Omega_{z+4,y,x}^t)
\end{aligned}$$

(d) 1st order in time 25-point variable-coefficient anisotropic stencil in three dimensions, with symmetry across each axis.

$$\begin{aligned}
& \text{for } t = 0 \text{ to } T - 1 \\
& \quad \text{for } z = 1 \text{ to } N_z \\
& \quad \quad \text{for } y = 1 \text{ to } N_y \\
& \quad \quad \quad \text{for } x = 1 \text{ to } N_x \\
& \quad \quad \quad \quad \Omega_{z,y,x}^{t+1} = 2 * \Omega_{z,y,x}^t - \Omega_{z,y,x}^{t-1} + \alpha_{z,y,x} * [w_0 * \Omega_{z,y,x}^t \\
& \quad \quad \quad \quad \quad + w_1 * ((\Omega_{z,y,x-1}^t + \Omega_{z,y,x+1}^t) + (\Omega_{z,y-1,x}^t + \Omega_{z,y+1,x}^t) + (\Omega_{z-1,y,x}^t + \Omega_{z+1,y,x}^t)) \\
& \quad \quad \quad \quad \quad + w_2 * ((\Omega_{z,y,x-2}^t + \Omega_{z,y,x+2}^t) + (\Omega_{z,y-2,x}^t + \Omega_{z,y+2,x}^t) + (\Omega_{z-2,y,x}^t + \Omega_{z+2,y,x}^t)) \\
& \quad \quad \quad \quad \quad + w_3 * ((\Omega_{z,y,x-3}^t + \Omega_{z,y,x+3}^t) + (\Omega_{z,y-3,x}^t + \Omega_{z,y+3,x}^t) + (\Omega_{z-3,y,x}^t + \Omega_{z+3,y,x}^t)) \\
& \quad \quad \quad \quad \quad + w_4 * ((\Omega_{z,y,x-4}^t + \Omega_{z,y,x+4}^t) + (\Omega_{z,y-4,x}^t + \Omega_{z,y+4,x}^t) + (\Omega_{z-4,y,x}^t + \Omega_{z+4,y,x}^t))]
\end{aligned}$$

(e) 2nd order in time 25-point constant-coefficient isotropic stencil in three dimensions, with symmetry across each axis.

Fig. 3.1: Examples of iterative stencil computations, starting with initial domain Ω^0 . The stencil operators in b, c, d, and e are analyzed in this paper. w represents scalar coefficients and W represents domain-sized coefficients.

In the following we describe in detail two “corner cases” of stencil update schemes: a three-dimensional seven-point stencil with constant coefficients (Jacobi-type smoother, see Fig. 3.1b) and a three-dimensional 25-point stencil with constant coefficients (see Fig. 3.1e). These examples were picked because they are simple to model for memory-bound situations but only the first is a good candidate for temporal blocking, as will be shown in the following two subsections. Later we will show the effectiveness of temporal blocking for the Jacobi smoother, the variable-coefficient 7-point stencil shown in Fig. 3.1c, and the variable-coefficient 25-point stencil shown in Fig. 3.1d.

3.3.1. Three-dimensional seven-point stencil with constant coefficients.

The standard two-grid three-dimensional “Jacobi” update scheme in Fig. 3.1b is probably the best analyzed stencil algorithm to date. From a data flow perspective the spatial loop nest reads one array ($\Omega[0][z][y][x]$) and updates another ($\Omega[1][z][y][x]$). In double precision, the minimum code balance is thus $B_C = 24$ bytes/LUP: eight bytes for loading one new element of the previous time step data, eight bytes for the write-allocate transfer on the new time step, and eight bytes for evicting the updated data back to memory. The write-allocate transfer may be avoided by the use of “non-temporal stores,” which bypass the memory hierarchy, thereby reducing the code balance to 16 bytes/LUP. Since this optimization is of minor importance for the practically relevant cases shown below, we will not discuss it here any further.

Depending on the grid size and the cache size, spatial blocking may be required to achieve the minimum code balance of 24 bytes/LUP. If three successive “layers” of size $N_x \times N_y$ grid points fit into a cache, the only load operation within a lattice site update that causes a cache miss goes to $\Omega[0][z+1][y][x]$, and all other loads can be satisfied from the cache. If C is the cache size, we assume (as a rule of thumb) that only about $C/2$ is available for the previous time step data, and the layer condition for double precision is

$$3 \times N_x \times N_y \times 8 \text{ bytes} < \frac{C}{2n_{\text{threads}}} . \quad (3.1)$$

This assumes that OpenMP parallelization is done along the z axis with static scheduling. If this condition is violated, at least the loads to $\Omega[0][z+1][y][x]$, $\Omega[0][z-1][y][x]$, and $\Omega[0][z][y+1][x]$ will cause cache misses, which leads to a code balance of 40 bytes/LUP. If the cache is too small to even hold three successive rows of the grid, the only loads that come from the cache will be to $\Omega[0][z][y][x-1]$ and to $\Omega[0][z][y][x]$. The code balance for this case is 56 bytes/LUP.

The layer condition (3.1) is independent of N_z . Hence, it is sufficient to introduce spatial blocking in the x and/or y dimensions in order to arrive at the minimum code balance. In practice one should try to keep the inner (x) block size larger than about one OS page in order to avoid frequent TLB misses and excess data traffic due to hardware prefetching [13]. Additionally, we use “static,1” OpenMP scheduling, which relaxes the layer condition to

$$(n_{\text{threads}} + 2) \times N_x \times N_y \times 8 \text{ bytes} < \frac{C}{2} , \quad (3.2)$$

since each thread shares both neighboring layers of its current z layer with its neighboring threads (except the first and the last thread, which only share one layer with their respective neighbor).

Note that the layer condition can be satisfied for any cache in the hierarchy if the block sizes are chosen appropriately; for memory-bound implementations one usually tries to establish it for the outer-level cache (OLC) to ameliorate the impact of the memory bandwidth bottleneck. In case of temporal blocking, however, the bottleneck may not be main memory and the smaller caches need to be taken into account. Since the overhead at block boundaries becomes significant at small block sizes, the optimum code balance is a goal that is all but impossible to achieve in this case.

Figure 3.2a shows the performance of the seven-point stencil algorithm in double precision on one Ivy Bridge chip with up to ten cores for a grid of 960^3 points (circles) and the memory bandwidth as measured by `likwid-perfctr` (triangles), together with the estimated saturated performance (solid line) and ideal scaling (dashed line). With appropriate spatial blocking the expected saturated performance as given by the roofline model is

$$P_{\text{roof}} = \frac{b_S}{B_C} = \frac{40 \text{ GB/s}}{24 \text{ bytes/LUP}} = 1.67 \text{ GLUP/s} . \quad (3.3)$$

The performance saturates at 6–7 cores, and the available memory bandwidth is utilized by up to 95%. Since there is strong saturation, we expect a strong benefit from temporal blocking.

3.3.2. Three-dimensional 25-point stencil with constant coefficients.

The considerations about layer conditions as shown above for the seven-point stencil apply in a similar way for long-range stencils. In the particular case of the algorithm shown in Fig. 3.1e, one sweep of the grid updates one array (read/modify/write) and reads two more arrays, one of which is accessed in a radius-four (semi-bandwidth of four) stencil pattern. The minimum code balance for double precision is thus $B_C = 32 \text{ bytes/LUP}$.

Due to the long-range stencil the layer condition is changed as compared to the previous case. With “static,1” scheduling, each thread can share the eight neighboring layers $\Omega[0][z-4][\][\] \dots \Omega[0][z-1][\][\]$ and $\Omega[0][z+1][\][\] \dots \Omega[0][z+4][\][\]$ with its eight neighboring threads (four in either z direction), but the top and bottom threads have less sharing. Consequently, the layer condition is

$$(n_{\text{threads}} + 8) \times N_x \times N_y \times 8 \text{ bytes} < \frac{C}{2} . \quad (3.4)$$

If this condition is fulfilled, $\Omega[z+4][y][x]$ is the only element from the stencil array that has to come from main memory.

Figure 3.2c shows the performance and memory bandwidth for ideal spatial blocking on a ten-core Ivy Bridge chip. The roofline model predicts an upper performance limit of

$$P_{\text{roof}} = \frac{b_S}{B_C} = \frac{40 \text{ GB/s}}{32 \text{ bytes/LUP}} = 1.25 \text{ GLUP/s} . \quad (3.5)$$

In contrast to the Jacobi-type stencil there is no clear saturation. The data transfers within the cache hierarchy and the execution of the loop code with data from the L1 cache take so much time that there is no sufficient pressure on the memory interface to saturate the bandwidth even with ten cores, which makes this stencil a bad candidate for temporal blocking unless there is an opportunity to save significant time with more efficient in-core execution. A thorough analysis of this effect would exceed the scope of this work and will be published elsewhere [24].

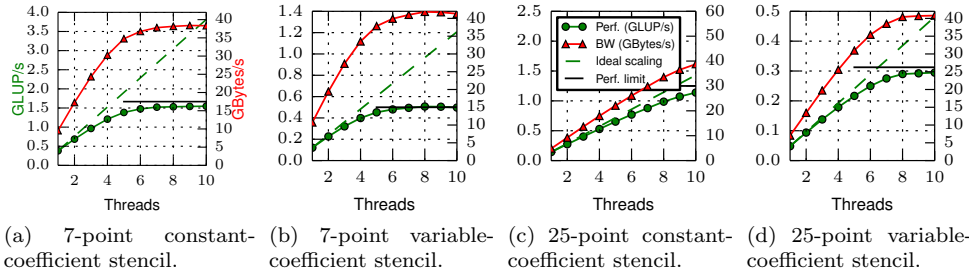


Fig. 3.2: Performance scaling across the cores of a chip with purely spatial blocking and data sets larger than L3 cache for the stencil algorithms shown in Fig. 3.1. Problem sizes: 960^3 , 680^3 , 960^3 , and 480^3 for subfigures a, b, c, and d, respectively. STREAM COPY memory bandwidth $b_S \approx 40$ GB/s.

3.3.3. Other stencils. Figures 3.2b and 3.2d show the saturation characteristics and maximum performance levels for the seven-point stencil with variable coefficients (ideal code balance of 80 bytes/LUP) and the 25-point stencil with axis-symmetric variable coefficients (ideal code balance of 128 bytes/LUP) listed in Figs. 3.1c and 3.1d, respectively. Both show strong saturation close to the performance levels predicted by the roofline model, and are thus viable targets for temporal blocking optimizations.

3.4. Upper performance bounds for in-cache execution. To find the expected performance of ideal temporal blocking (i.e., when performance has completely decoupled from the memory bottleneck), we have measured the performance at problems fitting completely in the last-level cache without temporal blocking. The results for the stencils discussed in the previous section are shown in Figs. 3.3a–3.3d. Problem sizes have been chosen so that work decomposition across threads is easy (no “artificial” load imbalance) and the inner loop length is not too short.

We see that all stencil algorithms scale very well across the cores, which is expected since the Ivy Bridge architecture does not have a hardware bottleneck except the main memory interface. It also shows that our implementation has no serious issues with OpenMP overhead or load balancing even with in-cache data sets.

4. Wavefront and diamond tiling temporal blocking.

4.1. Wavefront temporal blocking. Typical applications have larger grid size than a processor’s cache memory. If one sweep is completed before the next starts, each time step involves loading each grid point and writing the result from/to main memory. We call this the “naïve” approach. As a result, “naïve” stencil computations are typically memory-bound due to their low flops/byte ratio [6] (see Sect. 3 for a quantitative analysis). Temporal blocking alleviates the memory pressure by increasing the in-cache data reuse, i.e., several time step updates are performed to a grid point before evicting the data to main memory.

Figure 4.1a shows the naïve update order of a 3-point stencil in one dimension (see the pseudo-code in Fig. 3.1a). The fading gray color represents recently updated grid points, with the darkest assigned to the most recent update. The three “upward pointing” arrows in time steps three and four display the data dependency at each grid point, which is important to consider at temporal blocking optimizations. Wavefront

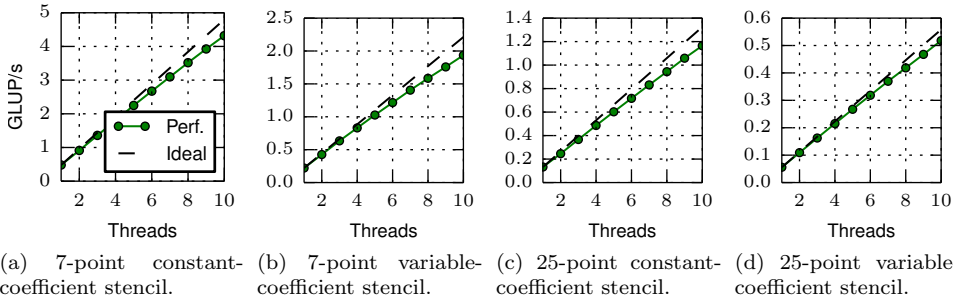
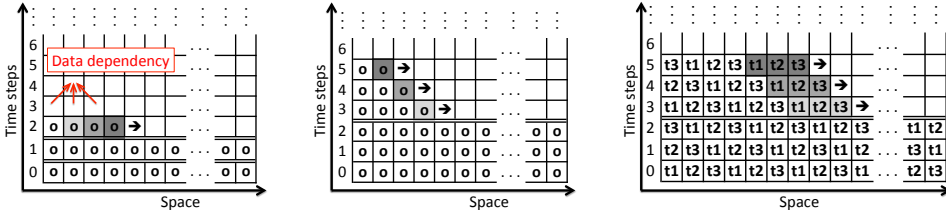


Fig. 3.3: Performance scaling across the cores of a chip without blocking and data sets fitting in the L3 cache for the stencil algorithms shown in Fig. 3.1. Problem sizes: $96 \times 96 \times 96$, $64 \times 64 \times 48$, $128 \times 64 \times 64$, and $64 \times 32 \times 32$ for subfigures a, b, c, and d, respectively. Smaller grids fit in L3 at variable-coefficient stencils because they require more bytes per grid point to hold the coefficients values.

temporal blocking is a well known technique in the literature [15, 31, 26]. Compared to the naïve approach, the grid points update order maximizes the reuse of the most recently visited grid points while respecting the data dependencies. Figure 4.1b shows the basic idea of wavefront temporal blocking for the 3-point stencil in one dimension. A wavefront line (“frontline”) traverses a space-time block in the direction of the arrows. The slope S of the frontline is determined by the radius of the stencil operator R , where higher order (i.e., longer range) stencils require a smaller frontline slope to respect the data dependency ($S = -1/R$). For example, the 3-point stencil has $S = -1$. The data in the frontline has to fit in the cache memory (along with the surrounding grid points touched by the stencil operator) to achieve the desired cache memory data reuse in the wavefront approach. The time dimension is blocked in a size that allows the frontline to fit in the desired cache. For example, three time steps are blocked in Figure 4.1b to illustrate the idea.

The wavefront can be executed sequentially (“1-thread wavefront”). On multi-core systems one can perform 1-thread wavefronts on separate space-time tiles, with no need (nor use) for any cache sharing among the threads. This approach was demonstrated in detail in [26].

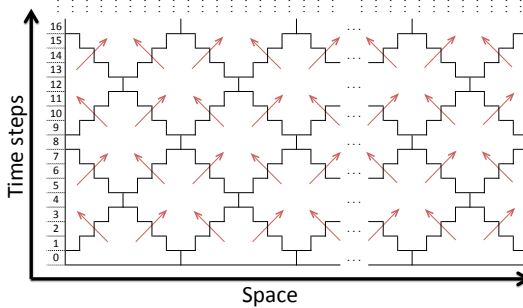
An explicitly multi-core aware wavefront scheme leveraging the shared cache among the threads was proposed in [29] (Similar concept in exploiting parallelism within the cache block was recently performed by Shrestha *et al.* [23]). In [29] approach the frontline update is pipelined over a group of threads sharing an outer-level cache. This has the advantage of reducing the memory bandwidth pressure and the total cache size requirement compared to the 1-thread wavefront. Figure 4.1c shows the multi-thread wavefront variant used in this paper: at each time step in the multi-frontline update, each thread performs an update of one or more grid points before proceeding to the next time step. All threads have to update the same number of frontlines for load balancing, and they must be synchronized after each time step update to ensure correctness. A global barrier is the simplest solution for this, but a relaxed synchronization scheme may result in better performance if the workload per thread is small [30].



(a) naïve: Lattice sites updated in chronological order, one time step at a time. Data dependencies example represented by red arrows. (b) Single thread wavefront traversal in space-time blocks. Frontlines are updated sequentially. (c) Multi-thread wavefront traversal in space-time blocks. One front-line update per thread, with thread synchronization after each time step update in the frontline.

Fig. 4.1: Different stencil update approaches for the 3-point stencil in one dimension. Fading gray boxes represent the last three updates.

Fig. 4.2: Diamond tiling on a one-dimensional space grid, with arrows representing inter-tile data dependencies. The number of diamond tiles per row represents the maximum attainable concurrency, as the tiles in the row can be executed independently of each other.



4.2. Diamond tiling. Diamond tiling has received much attention in recent years. Figure 4.2 shows the basic idea for the one-dimensional 3-point stencil. Arrows represent the data dependency across the diamond tiles. Diamond tiles that start at the same time step compose a “row of diamonds”, in which the diamond tiles are independent of each other. Each interior diamond tile has a data dependency on the two diamond tiles that share edges with it in the lower row of diamonds (“parents”). Half-diamond tiles at the boundaries of the spatial domain have only one parent. The slope of the tile edges depends on the stencil radius, where $S = \pm 1/R$. We consider atomic update of the diamond tiles in this work, i.e., a tile does not perform synchronization with other tiles until it is completely updated. Several advantages of diamond tiling make it favorable in shared memory systems: it maximizes the data reuse of the loaded data block [21], has low synchronization requirements, allows concurrent start-up in updating the diamond tiles, and uses a unified tile shape, which simplifies the implementation.

4.3. 1-thread wavefront diamond blocking. A multi-dimensional tiling algorithm called “cache accurate time skewing” (CATS) was proposed at [26]. They use space-time tiles larger than the cache size and employ wavefront temporal blocking inside the tiles to improve the data reuse in the cache memory (similar to [20, 29] in combining wavefront with large tiles). In CATS, the leading space dimension is not tiled and left for vectorization, while one other space dimension is used for wavefront and blocking (When running at more than one dimensional grid).

We are interested in the CATS2 variant, where “2” stands for diamond tiling in one dimension plus wavefront in another dimension. It is suitable for three-dimensional problems and for distributed memory parallelization, which will be described in Section 5. Figure 5.1a shows one extruded diamond block of the CATS2 algorithm applied to a three-dimensional problem. The wavefront traverses along the z dimension. The diamond tiling is performed across the y dimension, allowing the diamond tile to perform spatial blocking to satisfy the layer condition. The x dimension is left intact for efficient hardware data prefetching and minimum TLB misses. Hence, each grid point in Fig. 5.1a extends along the full x range.

5. Approach: multi-thread wavefront diamond blocking. The implementation of our approach can be found in [9]. We use it to produce the results of this work.

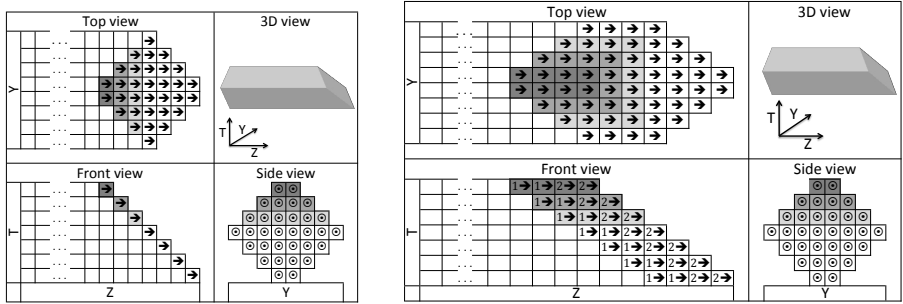
5.1. Tiling and threading scheme. The CATS2 algorithm has the advantage of efficiently utilizing the performance of multi-core processors with minimal thread synchronization and very efficient data reuse. However, we believe that two particular aspects of CATS can be potentially improved.

First, CATS2 relies on a large domain size in the diamond tiling dimension to have sufficient concurrency for the available threads. If this condition cannot be met, [26] proposes reverting to CATS1, which uses wavefront traversal in the same dimension of space-time parallelogram tiles. This prevents the CATS algorithm from taking advantage of diamond tiling as an efficient domain decomposition strategy in distributed memory. They also propose using higher-dimensional tiling to extract parallelism for many-core processors, which can increase the code complexity. Moreover, with the emergence of many-core architectures like the Intel Xeon Phi, it would be difficult to find sufficient concurrency for 60–240 threads in a reasonable grid size.

Second, no cache sharing among threads is assumed in the CATS2 algorithm, so each thread requires space in the cache memory and bandwidth from main memory for its own use. As a result, memory-starved stencil computations run out of cache and memory bandwidth, as will be shown in the results section. Moreover, it is unclear whether the cache size and memory bandwidth per thread as seen in contemporary multi-core designs will be available in future architectures. For example, the Intel Xeon Phi has 128KiB and 8KiB cache per thread in the L2 and L1 caches, respectively, and it achieves only about 3GB/s per core of memory bandwidth in full saturation. A temporal blocking scheme should be flexible enough to accommodate such hardware limitations if required.

We propose an approach that reduces the cache size and memory bandwidth requirements and reduces the concurrency limitations while retaining the advantages of CATS2. The basic idea is to use the multi-threaded wavefront temporal blocking proposed in [29] in place of the CATS2 1-thread wavefront. We call our concept multi-threaded wavefront diamond blocking (MWD), where CATS2 is a special case with 1-thread wavefront diamond blocking (1WD). Figure 5.1b shows one block of the MWD algorithm. Load-balancing is important here as the number of stencil updates in the frontline varies across time steps according to the diamond width. The multi-thread wavefront updates are performed in the same manner as described in Sect. 4.1. The parallelization of each time step of the multi-frontline update ensures load balancing among the threads.

Threads are assigned to the extruded diamond in groups (“thread groups”). For example, two-threads wavefront diamond blocking (2WD) is used in Figure 5.1b.



(a) Diamond tiling with a single-thread wavefront (similar to CATS2) in a three-dimensional space grid using a single frontline.

(b) Diamond tiling with a multi-thread wavefront (shown here with two threads) in a three-dimensional space grid, using two frontlines per thread.

Fig. 5.1: Diamond tiling with wavefront temporal blocking.

Multiple thread groups can run concurrently, working on different diamond tiles and respecting inter-diamond dependencies.

One advantage of MWD over CATS2 is controllable cache sharing among the threads. When multiple threads update an extruded diamond together, they share the memory bandwidth and the cache memory block, reducing the pressure on these resources. Moreover, less concurrency is required across multiple diamonds (i.e., in the y dimension), since some concurrency is moved to the wavefront dimension. This allows for smaller domain sizes without sacrificing concurrency.

Threads can be scheduled to the extruded diamonds in a variety of ways. Orozco *et al.* [21] use global synchronization after each row of diamonds update to respect the inter-diamond dependencies. The diamond tiles in [26] are preassigned to threads before starting the stencil computations, taking the inter-diamond data dependency during tile updates into account. These approaches are sufficient to avoid idling threads as long as the workload is balanced. Workload variation can result from domain boundary handling: In this work, diamond tiles at the boundary of the sub-domain exchange data and synchronize with neighbor processes. This causes load imbalance in processing diamond tiles, which varies according to the used network interconnect. To resolve this issue, we schedule the diamond tiles dynamically to the thread groups. A FIFO queue maintains a list of available tiles for update. When a thread has completed updating a tile, it pushes its dependent diamond tile(s) to the queue if those tiles have no other unmet dependencies. “Pop” operations are performed to assign available tiles to thread groups. The FIFO queue is protected from concurrent updates by an OpenMP critical region. Since the queue updates are performed infrequently, the synchronization overhead is negligible.

Proper choices of the diamond tile size and the number of multi-frontline updates are crucial for good performance. In particular, maximizing the diamond tile size in the L3 cache increases the data reuse in the L3 cache. The diamond tile size in [26] is computed based on the processor’s cache memory size and the stencil operator specification. This approach does not guarantee best cache utilization to maximize the data reuse. The optimal cache block size can vary based on the cache memory architectural features, such as associativity, and the data access patterns of the used

stencil operator. Auto-tuning is used in this work to select the diamond tile size and number of multi-frontline wavefront updates. The parameter search space is narrowed down to diamond tiles that fit within a predefined cache size range. The cache block size is computed based on diamond size, number of wavefronts, grid size, and stencil type, as will be described in Section 5.3. Several constraints are considered in selecting valid cache block size, for example, having sufficient concurrency and integer number of diamond tiles in each row of diamond tiles.

5.2. Distributed-memory parallelization. Parallelizing stencil computations over distributed memory nodes is quite straightforward if no temporal blocking is involved. Each time step update is followed by halo data communication. In such a bulk-synchronous scheme, strong scalability is naturally limited by data transfer overhead. A partial remedy is provided by the halo-first update scheme, in which domain boundaries are updated first, and then asynchronous message passing is performed while updating the bulk of the domain.

Distributed memory parallelization can be combined with diamond tiling as shown in Figure 5.2. The arrows represent the data dependencies across subdomains, and the same number of adjacent tiles is assigned to each process except the rightmost one (largest y coordinate). To maintain load balance in terms of computation and communication, the leftmost half diamond tile is assigned to the rightmost process. Regular diamond tiles are used at the boundary of subdomains, with the difference of performing communication before and after the tile update. Thread groups handling boundary diamond tiles are blocked until their MPI communication is complete. Extra delay can occur if no thread group is updating the diamond tile at the other end of the communication. Adding priority in scheduling the tiles at the boundary to thread groups can alleviate this issue, which is left for future work.

Since domain decomposition is performed along the middle space dimension (y), the boundary data to be communicated does not reside in contiguous memory locations. User-defined strided MPI data types are not efficient in our multi-threaded implementation, as MPI implementations handle the required packing/unpacking operations purely sequentially. We use explicit multi-threaded halo data packing/unpacking to resolve this issue.

Diamond tiling offers several advantages in distributed memory parallelization. The tessellation of the diamond tiles allow using a unified tile structure everywhere. It also allows maximum stencil updates in space-time without relying on exchanging boundaries with neighbor processes after each grid sweep. Finally, there is a natural overlap of computation with communication. Communication does not block all threads, and no thread has to be sacrificed for asynchronous communication. Threads can handle communication or perform stencil updates as needed.

5.3. Wavefront diamond blocking cache block size requirement. Four parameters are used to calculate the cache block size of the wavefront: the diamond width D_w in the y axis, the number of additional wavefront frontlines N_F , the number of bytes in the x axis N_{xb} , and the stencil operator properties (see below). The wavefront width W_w is determined by the diamond width and the number of frontlines: $W_w = D_w + N_F - 1$. The stencil operator properties include the stencil radius. For example, the 7- and 25-point stencils have $R = 1$ and $R = 4$, respectively. They also include the number of additional domain-sized streams used in the stencil operator, N_D . For example, the 7-point stencil with constant coefficients uses two domain-sized streams (Jacobi style update). The 7-point stencil with variable coefficients uses seven additional domain-sized streams to hold the coefficients. Total number of

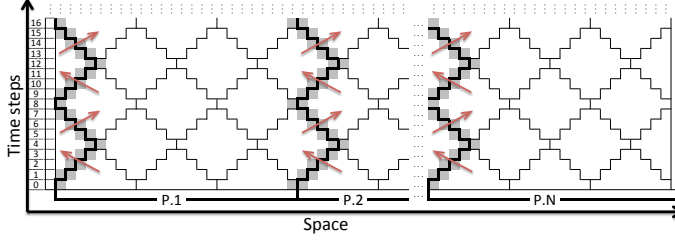


Fig. 5.2: Distributed memory parallelization with diamond tiling for a one-dimensional space grid. Arrows represent the data dependencies across subdomains. The leftmost column of half diamonds is assigned to the rightmost process to achieve load balance in computation and communication.

bytes required in the cache block for a stencil with $R=1$, with some approximations, is:

$$N_{xb} \cdot \left[N_D \cdot \left(\frac{D_w^2}{2} + D_w \cdot N_F \right) + 2 \cdot (D_w + W_w) \right]. \quad (5.1)$$

Here, N_{xb} is the size of the “untiled” leading dimension, and $D_w^2/2 + D_w \cdot N_F$ is the diamond area in the y - z plane as shown in the top view of Figures 5.1a and 5.1b. The perimeter of the rectangle containing the cache block in the y - z plane is $2 \cdot (D_w + W_w)$. For example, we have $D_w = 8$ and $N_F = 0$ in Figure 5.1a, so $W_w = 8 - 1 + 0 = 7$ and the total block size is $N_{xb} \cdot ((8^2/2 + 8 \cdot 0) + 2 \cdot (8 + 7)) = 70 \cdot N_{xb}$ bytes. Figure 5.1b differs with $N_F = 3$, so $W_w = 8 - 1 + 3 = 10$ and the cache block size is $N_{xb} \cdot ((\frac{8^2}{2} + 8 \cdot 3) + 2 \cdot (8 + 10)) = 92 \cdot N_{xb}$ bytes.

Higher-order stencils (with $R > 1$) have a steeper frontline slope in the wavefront to satisfy the data dependency across time steps. This results in different wavefront lengths ($W_w = D_w - 2 \cdot R + N_F + 1$). Also the required cache block size changes as follows:

$$N_{xb} \cdot \left[N_D \cdot D_w \cdot \left(\frac{D_w}{2} - R + N_F + 1 \right) + 2 \cdot R \cdot (D_w + W_w) \right]. \quad (5.2)$$

Examples of wavefront cache block size requirements for the 7-point constant-coefficient and the 25-point variable-coefficient stencils are shown in Figure 5.4. Considering that each thread group requires a separate cache block, the 25-point stencil with variable coefficients needs a lot of cache on modern multi-core processors, even at the smallest diamond tile size. When using the 1WD algorithm on a ten-core CPU, 50 MiB of cache memory are required, which is beyond the capacity of current designs. On the other hand, the 7-point stencil with constant coefficients can be used with a sufficiently large diamond tile size and still fulfill the cache demand even with 1WD. Since each data set in Fig. 5.4 represents the cache size for only one thread group, it is evident that, all other parameters being equal, MWD allows for larger tile sizes than 1WD.

6. Results. In this section we compare the performance of spatially blocked code with our MWD variants. On the ten-core Intel Ivy Bridge processor, four thread group sizes are investigated: 1WD, 2WD, 5WD, and 10WD. Since we perform parameter

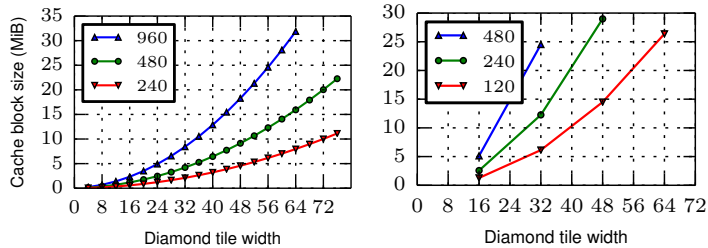


Fig. 5.4: Model of MWD cache block size requirements per thread group at different diamond tile sizes. Each data set corresponds to a different grid size.

(a) 7-point stencil with constant coefficients stencil. (b) 25-point stencil with variable coefficients stencil.

auto-tuning and dynamic scheduling of diamond tiles to threads, our 1WD approach is an improved version of CATS2.

We show performance results for those stencils that were analyzed in the previous sections and shown to be strongly memory bound so that temporal blocking is a viable optimization: 7-point constant-coefficient (Fig. 3.1b), 7-point variable-coefficient (Fig. 3.1c), and 25-point variable-coefficient (Fig. 3.1d).

Three sets of results are presented: OpenMP thread scaling performance on a single socket (Sect. 6.1), increasing cubic grid size performance in a single socket (Sect. 6.2), and distributed memory strong scaling performance (Sect. 6.3). For all performance results we chose the grid size that fits in 32 GiB of memory, which is the memory size per socket in the benchmark system.

6.1. Thread scaling performance. Although we present scaling runs from 1 to 10 threads on an Intel Ivy Bridge socket, with fixed grid size, auto-tuning is performed at 10 threads only. To further improve the results, a brute-force parameters search is performed at the 10 threads experiments for better results. For each of the thread scaling results, the same diamond width and number of frontlines of the corresponding 10-threads experiment is used.

6.1.1. 7-point stencil with constant coefficients. All thread scaling results are shown in Figures 6.1a and 6.1d.

As shown in Figure 6.1a, 1WD achieves a $2.6\times$ speedup compared to spatially blocked code, with about 92% threads parallel efficiency and 95% of the in-L3 performance (see Fig. 3.3a) using 10 cores. 2WD, 5WD, and 10WD achieve 4%, 8%, and 12% less performance compared to 1WD, respectively. Since all MWD variants are decoupled from main memory, the core performance and the intra-cache data transfers become the bottleneck. The 1WD implementation has some advantage here since it does not require OpenMP parallelism in the wavefront update, and the OpenMP barrier overhead increases at larger thread groups.

In terms of memory bandwidth usage, as shown in Figure 6.1d, 1WD, 2WD, 5WD, and 10WD save about 40%, 39%, 63%, and 68% of the memory bandwidth, respectively. 10WD requires roughly 47% less memory bandwidth compared to 1WD, which makes it a better candidate on future, more bandwidth-starved architectures: Since 10WD uses 32% of the available memory bandwidth, it can theoretically maintain the same performance on processors with a bandwidth that is a factor of three lower than on the benchmark system (assuming the same core performance). This result also raises expectations of 10WD showing more benefit or stencils with a higher code balance (see below).

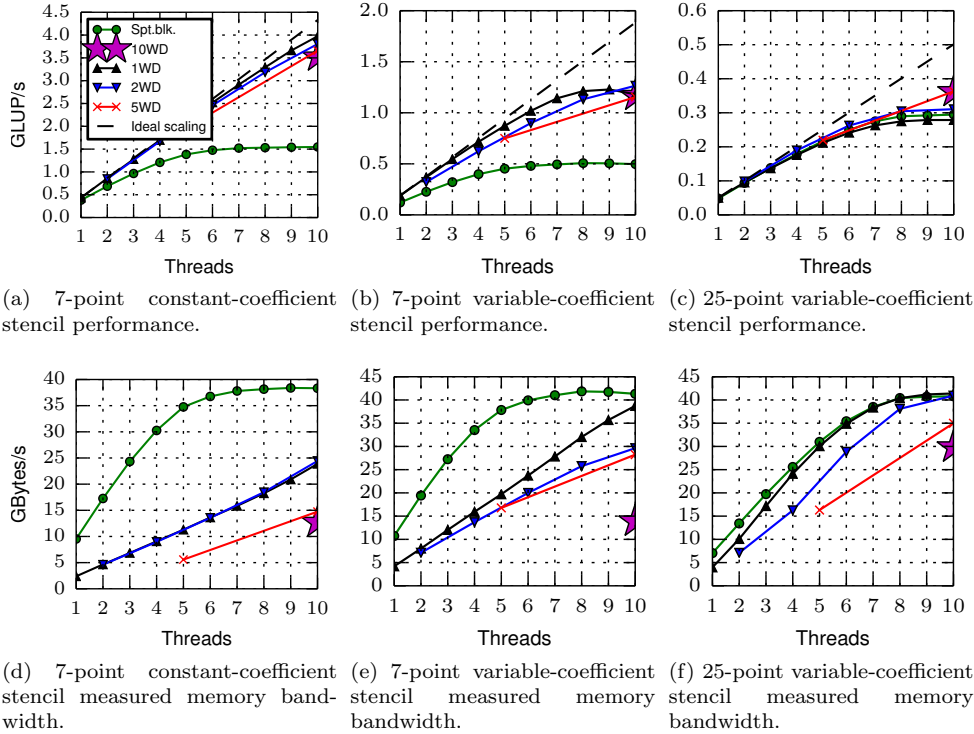


Fig. 6.1: Performance (top row) and memory bandwidth (bottom row) scaling vs. number of threads of three stencil types (columns) on a 10-core Intel Ivy Bridge socket. Problem sizes: 960^3 , 680^3 , and 480^3 for 7-point constant-coefficient, 7-point variable-coefficient, and 25-point variable-coefficient, respectively. Ideal scaling is based on 1 thread 1WD performance at the three stencil types.

In Table 6.1 we show power dissipation and energy to solution measurements taken with `likwid-perfctr` (which uses the RAPL facility available in modern Intel processors). When considering aggregate DRAM and processor power, 10WD draws 13% less power compared to 1WD, which is mostly due to reduced DRAM bandwidth usage. Due to its slightly lower performance, 10WD can still not achieve significant energy savings compared to 1WD. However, future architectures are expected to show a much larger contribution to overall power from memory transfers, which will make MWD approaches more attractive also in terms of energy consumption. Note also that all variants with temporal blocking dissipate more power on the CPU but less in the DRAM compared to spatial blocking. Together with the much improved time to solution this results in considerable energy savings, even when running the spatially blocked version with only six cores, i.e., at the performance saturation point. For code with saturating performance characteristics, this is the point with minimal energy to solution [12].

A more detailed energy consumption analysis is left to future work.

6.1.2. 7-point stencil with variable coefficients. All thread scaling results are shown in Figures 6.1b and 6.1e.

	Method	Spt. Blk.		1WD	2WD	5WD	10WD
	Threads	10	6	10	10	10	10
Power [W]	CPU	52.9	44.1	58.5	59.0	57.4	56.6
	DRAM	42.5	39.8	32.6	33.5	24.4	22.4
	Total	95.4	83.9	91.1	92.4	81.7	79.0
Energy [J]	CPU	33.9	29.6	14.7	15.5	15.8	16.2
	DRAM	27.3	26.8	8.2	8.8	6.7	6.4
	Total	61.2	56.4	22.9	24.4	22.5	22.7

Table 6.1: Power dissipation and energy to solution for the 7-point stencil with constant coefficients on a 10-core Intel Ivy Bridge socket at a grid size of 960^3 .

2WD achieves the best performance, as shown in Figure 6.1b, with a speedup of about $2.55\times$ compared to spatially blocked code. The performance saturation and decay of 1WD beyond 7 threads deserves an explanation. Since the memory bandwidth scales almost linearly up to 10 threads, one must conclude that the code balance increases. Experiments with half the inner domain size (i.e., $340\times 680\times 680$) show that scaling continues up to 10 threads, topping at about 1.5 GLUP/s. It turns out that for 1WD the required cache block size at ten threads is very close to the available cache size at the selected diamond size (see Sec. 6.1.4 for details). This problem can be remedied by split tiling in the leading dimension, which we leave for future work.

2WD, 5MWD, and 10WD decouple from main memory, saving up to about two thirds of the memory bandwidth in case of 10WD.

Similar memory bandwidth usage of 2WD and 5WD is measured in Figure 6.1e because the same diamond tile size ($D_w = 8$) is selected by the auto-tuner, compared to 10WD that has a larger diamond tile size ($D_w = 20$). 5WD has the same diamond tile size as 2WD in this case because the next larger valid diamond size would require more cache than is available.

6.1.3. 25-point stencil with variable coefficients. All thread scaling results are presented in Figures 6.1c and 6.1f.

Since this stencil has a very large code balance of 120 bytes/LUP, we expect larger thread groups to perform better. The memory bandwidth of the spatial blocking, 1WD, and 2WD codes cannot decouple from memory and saturate at eight threads, as shown in Figure 6.1f. On the other hand, 5WD and 10WD save roughly 12.5% and 25.5% of the memory bandwidth, respectively, which allows them to have scalable performance as shown in Figure 6.1c. 5WD and 10WD achieve about $1.23\times$ speedup compared to the spatially blocked code.

The 1WD algorithm achieves worse performance compared to spatially blocked code due to cache capacity misses, since it requires 93 MiB of cache even at the smallest possible diamond tile size.

6.1.4. Thread scaling diamond tile size analysis. The 7-point stencil with constant coefficients achieves the best performance with $D_w = 12$ at 1WD and 2WD. Although 2WD has less cache size and memory bandwidth requirements than 1WD, it uses the same diamond width because the next larger diamond width ($D_w = 16$) does not fit in the L3 cache. 2WD requires 25.4MiB cache block size at $D_w = 16$ compared to 17.5MiB at $D_w = 12$, so $D_w = 16$ can cause a lot of capacity misses to

the main memory. The best performance at 5WD and 10WD is achieved at $D_w = 24$. Figure 6.1d shows that the same memory bandwidth usage is obtained when the same diamond width is used.

The 7-point stencil with variable coefficients uses $D_w = 8$ at 1WD, 2WD, and 5WD, and $D_w = 20$ at 10WD. 1WD uses more memory bandwidth than 2WD and 5WD, although they have the same code balance. The best performance in 1WD is obtained at a diamond width that causes many capacity misses to main memory, because the selected cache block size is large. Although the next smaller diamond width ($D_w = 4$) can avoid these cache misses in 1WD, it achieves lower performance due to the higher code balance. 1WD has similar memory bandwidth usage to 2WD and 5WD at eight threads, where the cache block size does not cause many cache capacity misses.

The 25-point stencil with variable coefficients uses $D_w = 16$ at 1WD, 2WD, and 5WD, and $D_w = 32$ at 10WD. The cache block size at 1WD and 2WD is larger than the available cache size even with smallest possible diamond width ($D_w = 16$), causing the memory bandwidth to saturate in these cases.

6.2. Performance at increasing grid size. Here we compare the performance of problems with increasing cubic grid size. The grid size in each dimension is set to a multiple of 64.

Performance and memory bandwidth measurements are shown in Figures 6.2. In all cases with temporal blocking, but especially for the 7-point stencil with variable coefficients, a gradual decline of performance with growing grid size can be observed. This can be attributed to the same cause as the bad thread scaling for 1WD beyond 7 threads in Fig. 6.1a.

6.2.1. 7-point stencil with constant coefficients. All results are shown in Figures 6.2a and 6.2d.

1WD achieves the best performance at most of the grid sizes, as it decouples from main memory and does not have the OpenMP overhead in the kernel, which is described in the thread scaling results. The MWD achieves similar relative performance to 1WD as in the thread scaling results. Also, larger thread groups consistently use less memory bandwidth at all domain sizes as seen in Figure 6.2d.

The observed fluctuations in the performance are the results of the variation in the selected diamond tile sizes at different grid sizes. The requirement of having an integer number of diamond tiles in the row of diamonds prevents the autotuner from selecting the optimal diamond size. Instead, it selects the nearest smaller diamond size that allows integer number of diamonds in the given grid size.

In contrast to spatial blocking and 1WD, the other algorithms do not achieve high performance for in-cache domain sizes. This is mainly due to the OpenMP synchronization overhead, which becomes significant at small problem sizes, and also probably due to the high data sharing among the threads, which results in invalidating many lines in the private caches.

6.2.2. 7-point stencil with variable coefficients. All results are shown in Figures 6.2b and 6.2e.

All the MWD approaches achieve similar performance at all grid sizes. 1WD outperforms the other variants at most of grid sizes up to a domain size of 512^3 , then 2WD takes the lead.

6.2.3. 25-point stencil with variable coefficients. All results are shown in Figures 6.2c and 6.2f.

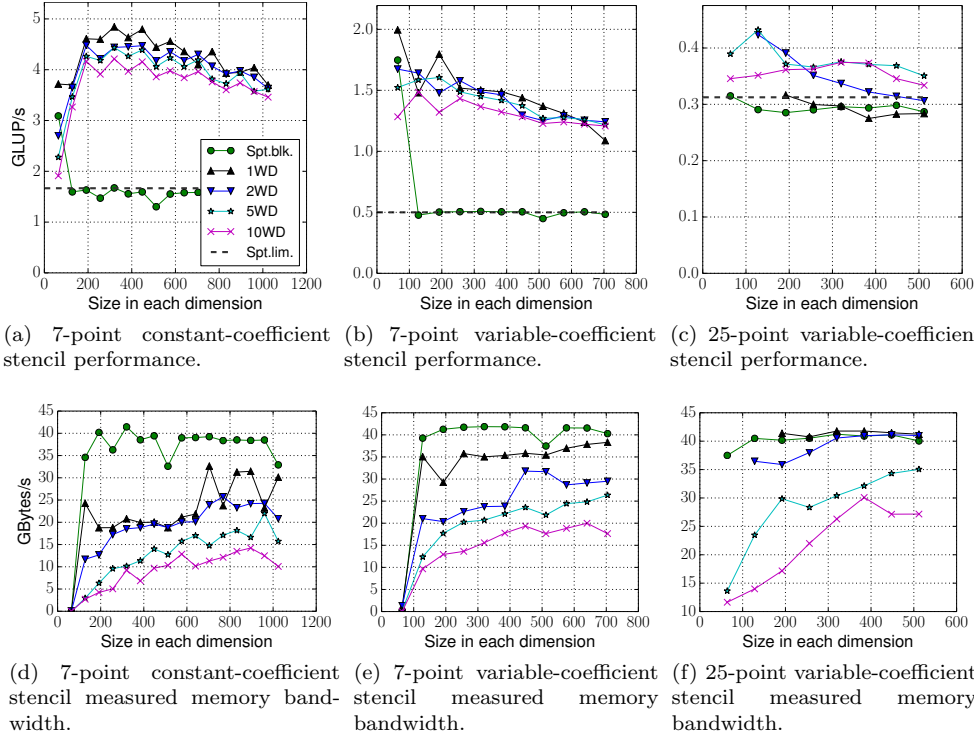
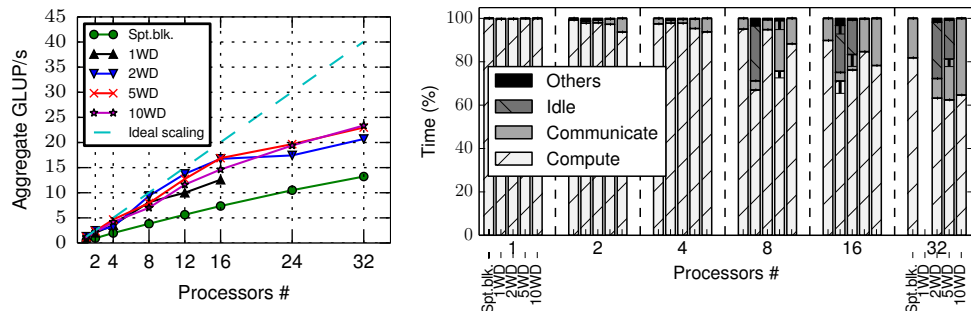


Fig. 6.2: Performance (top row) and memory bandwidth (bottom row) vs. grid size of three stencil types (columns) on a 10-core Intel Ivy Bridge socket. At 7-point constant-coefficient stencil, all MWD algorithms achieve between $2\times$ and $3\times$ speedup compared to the spatially blocked code, with 10WD using less than one third of the available memory bandwidth.

1WD does not have results at small domain sizes because there is no sufficient concurrency for all the available threads, even with the smallest diamond size ($D_w = 16$). 2WD achieves the best performance up to domain size 192^3 , where it starts hitting the memory bandwidth limit at larger grid sizes.

The performance-optimal diamond width selected by the auto-tuner varies with stencil type and grid size. Smaller grid sizes tend to get larger diamond tiles, as the leading dimension size is smaller. Stencils with variable coefficients have larger storage requirements per grid point, which limits the size of the performance-optimal diamond tile. At experiments with $N > 100$, the median diamond width ranged between 16 and 32 at the 7-point constant-coefficient, between 8 and 16 at the 7-point constant-coefficient, and between 16 and 32 at the 25-point variable-coefficient stencil.

6.3. Distributed memory strong scaling performance. Strong scaling performance experiments were performed for the 7-point variable-coefficient and 25-point variable-coefficient stencils. We present only the 7-point results here because they are not qualitatively different from the 25-point case. Domain decomposition across the y axis is achieved through MPI message passing, as described in Sect. 5.2. An Intel



(a) Performance. Ideal scaling based on 2WD performance at single process. (b) Time distribution. Error bars with standard deviation under 3% are suppressed.

Fig. 6.3: Distributed memory strong scaling performance of the 7-point stencil with variable coefficients at a grid size of 768^3 . A full 10-core Intel Ivy Bridge socket was used per MPI process.

Ivy Bridge socket is assigned to each MPI process, using ten OpenMP threads per socket. All results are shown in Figure 6.3.

1WD does not work beyond 16 processes because smaller subdomains in the y axis cannot provide sufficient concurrency to run all the available threads (“concurrency condition”). To run 1WD at 24 MPI processes the minimum subdomain size would be 4 [min. diamond width] \times 10 [threads/process] \times 24 [processes] = 960 grid points along the y axis. Other MWD algorithms have less concurrency requirements in the diamond tiling dimension, as another dimension of concurrency is introduced in the wavefront blocking direction. The concurrency condition can be satisfied at 2WD, 5WD, and 10WD using 50%, 20%, and 10% of the minimum grid size that satisfies the concurrency condition at 1WD.

2WD achieves less performance compared to 5WD and 10WD at 24 and 32 processes due to the restrictions imposed by the concurrency condition, which limits 2WD to small diamond tile sizes ($D_w = 4$ at 24 and 32 processes, compared to $D_w = 8$ at 16 processes). On the other hand, 5WD and 10WD can use larger tile sizes while satisfying the concurrency condition. For example, 5WD and 10WD use $D_w = 12$ and $D_w = 24$, respectively, at 32 processes. The same concurrency limitation causes the performance of 1WD to drop at 12 and 16 processes, where $D_w = 4$ compared to $D_w = 8$ at 8 processes.

Timing routines are used in the code to profile the major parts. As shown in Figure 6.3b, the run time is mainly spent in performing stencil updates (“Compute”), communicating the halo data across MPI processes (“Communicate”), and thread groups idle time when the task queue is empty in the MWD implementation (“Idle”). Thread groups can have different time distribution as they perform their tasks independently from each other. Error bars are used in Figure 6.3b to present the standard deviation of the thread groups’ run time for each component.

When the concurrency limit is approached in the MWD implementation, the idle time percentage increases, as can be seen in Figure 6.3b. For example, the subdomain of 1WD at 16 processes has 12 diamond tiles in the row ($N_y/(D_w \times P) = 768/(4 \times 16) = 12$ diamond tiles/row, where P is the number of processes), which is very close to the concurrency limit of the ten thread groups. Handling boundary tiles takes more time

compared to interior tiles because of the data exchange. When the interior diamond tiles of a row are updated before the boundary tiles, less concurrency will be available. This causes some thread groups to remain idle when the subdomain size is near the concurrency limit.

As shown in Figure 6.3a, the MWD implementation scales well up to 16 processes. The large surface-to-volume ratio of the subdomains at 24 and 32 processes results in large communication overhead, as shown in Figure 6.3b. Performing domain decomposition at additional dimensions would allow the code to have scalable performance at more processes, which is left for the future work.

7. Conclusion and future work. In this work we have combined the concepts of diamond tiling and multi-core aware temporal wavefront blocking to construct multi-threaded wavefront diamond blocking (MWD), a new temporal blocking scheme for improving the performance of stencil computations on contemporary multi-core CPUs. Using three different stencil types (short range with constant coefficients, short range with variable coefficients, and long range with variable coefficients) we have demonstrated that our solution exerts considerably less pressure on the memory interface for all stencils considered compared to single-thread diamond tiling. It is also more flexible in terms of assigning parallel resources to grid tiles since multiple threads work concurrently on updates within a diamond tile using the shared cache. Finally, the cache size requirements are also reduced. However, depending on the diamond tile size, OpenMP and synchronization overhead may be relevant, although we use a relaxed synchronization scheme that avoids global barriers across tiles. MPI-based distributed-memory parallelization of the MWD scheme is free of global synchronization and lends itself to natural overlapping of computation and communication.

Performance results on a modern 10-core Intel CPU show that MWD can outperform single-thread diamond tiling when the code balance of the purely spatially blocked code is large (such as for a 25-point long-range stencil with variable coefficients). Future, more bandwidth-starved architectures will benefit even more strongly from the reduced pressure on the memory interface. We have also shown that the energy consumption in the DRAM is considerably smaller with MWD, leading to savings in energy to solution even if there is no performance gain.

These results open the possibility for future work in multiple directions. First of all, our MPI implementation still suffers from idle threads when boundary tiles in an MPI process are updated late. This could be corrected by giving these tiles higher priority within the subdomain. Furthermore, the one-dimensional domain decomposition limits strong scalability and leads to a performance decay for large problem sizes. It should be improved by introducing tiling in the other dimensions.

Some possible optimizations are marginal on mainstream multi-core CPUs but may be decisive on future many-core CPUs like the Intel Xeon Phi, where thread synchronization is costly and efficient SIMD vectorization is absolutely required. Although some steps have already been taken to reduce thread synchronization overhead, barriers are still used inside the multi-core wavefront to ensure correctness. These could be eliminated by a relaxed synchronization scheme along the lines of Wittmann *et al.* [30]. Finally, alignment optimizations and data layout transformations could be imposed to allow for fully aligned data accesses and thus enable more efficient SIMD vectorization.

The implications of performance and memory transfer volume for power dissipation and energy to solution have as yet not been investigated thoroughly. As shown

in Sect. 6.1.1, the MWD algorithms show interesting power behavior because it is possible to end up in a situation where energy to solution is minimal at a non-optimal performance. Detailed energy models like the model introduced by Choi *et al.* [3] may lead to valuable insights concerning this issue.

Acknowledgments. The Extreme Computing Research Center at KAUST supported T. Malas. Part of this work was supported by the German DFG priority programme 1648 (SPPEXA) within the project Terra-Neo, and by the Bavarian Competence Network for Scientific High Performance Computing in Bavaria (KONWIHR) under project OMI4papps.

REFERENCES

- [1] V. BANDISHTI, I. PANANILATH, AND U. BONDHUGULA, *Tiling stencil computations to maximize parallelism*, in Proceedings of the International Conference for High Performance Computing, Networking, Storage and Analysis, Nov 2012, pp. 1–11.
- [2] U. BONDHUGULA, A. HARTONO, J. RAMANUJAM, AND P. SADAYAPPAN, *A practical automatic polyhedral parallelizer and locality optimizer*, ACM SIGPLAN Notices, 43 (2008), pp. 101–113.
- [3] J. W. CHOI, D. BEDARD, R. FOWLER, AND R. VUDUC, *A roofline model of energy*, in International Parallel and Distributed Processing Symposium, Washington, DC, USA, 2013, IEEE Computer Society, pp. 661–672.
- [4] M. CHRISTEN, O. SCHENK, AND H. BURKHART, *PATUS: A code generation and autotuning framework for parallel iterative stencil computations on modern microarchitectures*, in International Parallel and Distributed Processing Symposium, May 2011, pp. 676–687.
- [5] K. DATTA, *Auto-tuning Stencil Codes for Cache-Based Multicore Platforms*, PhD thesis, EECS Department, University of California, Berkeley, Dec 2009.
- [6] K. DATTA, S. KAMIL, S. WILLIAMS, L. OLIKER, J. SHALF, AND K. YELICK, *Optimization and performance modeling of stencil computations on modern microprocessors*, SIAM Review, 51 (2009), pp. 129–159.
- [7] H. DURSUN, M. KUNASETH, K. NOMURA, J. CHAME, R. F. LUCAS, C. CHEN, M. HALL, R. K. KALIA, A. NAKANO, AND P. VASHISHTA, *Hierarchical parallelization and optimization of high-order stencil computations on multicore clusters*, The Journal of Supercomputing, 62 (2012), pp. 946–966.
- [8] M. FRIGO AND V. STRUMPEN, *Cache oblivious stencil computations*, in Proceedings of the 19th Annual International Conference on Supercomputing, New York, NY, USA, 2005, ACM, pp. 361–366.
- [9] *Girih stencil optimization framework*. https://github.com/tareqmalas/girih/releases/tag/SISC_submission2014.
- [10] T. GROSSER, A. COHEN, J. HOLEWINSKI, P. SADAYAPPAN, AND S. VERDOOLAEGE, *Hybrid hexagonal/classical tiling for gpus*, in Proceedings of Annual IEEE/ACM International Symposium on Code Generation and Optimization, ACM, 2014, p. 66.
- [11] T. GROSSER, S. VERDOOLAEGE, A. COHEN, AND P. SADAYAPPAN, *The relation between diamond tiling and hexagonal tiling*, Parallel Processing Letters, 24 (2014), p. 1441002.
- [12] G. HAGER, J. TREIBIG, J. HABICH, AND G. WELLEIN, *Exploring performance and power properties of modern multi-core chips via simple machine models*, Concurrency and Computation: Practice and Experience, (2014).
- [13] G. HAGER AND G. WELLEIN, *Introduction to High Performance Computing for Scientists and Engineers*, CRC Press, 2010.
- [14] T. HENRETTY, R. VERAS, F. FRANCHETTI, L. N. POUCHET, J. RAMANUJAM, AND P. SADAYAPPAN, *A stencil compiler for short-vector SIMD architectures*, in Proceedings of the 27th international ACM conference on International conference on supercomputing, ACM, 2013, pp. 13–24.
- [15] L. LAMPORT, *The parallel execution of do loops*, Communications of the ACM, 17 (1974), pp. 83–93.
- [16] *LIKWID performance tools*. <http://code.google.com/p/likwid>.
- [17] N. MARUYAMA, T. NOMURA, K. SATO, AND S. MATSUOKA, *Physis: an implicitly parallel programming model for stencil computations on large-scale GPU-accelerated supercomputers*, in Proceedings of the International Conference for High Performance Computing, Networking, Storage and Analysis, IEEE, 2011, pp. 1–12.

- [18] J. D. McCALPIN, *STREAM: Sustainable memory bandwidth in high performance computers*, tech. report, University of Virginia, Charlottesville, VA, 1991-2007. A continually updated technical report.
- [19] ———, *Memory bandwidth and machine balance in current high performance computers*, IEEE Computer Society Technical Committee on Computer Architecture Newsletter, (1995), pp. 19–25.
- [20] A. NGUYEN, N. SATISH, J. CHHUGANI, C. KIM, AND P. DUBEY, *3.5-D blocking optimization for stencil computations on modern CPUs and GPUs*, in Proceedings of the International Conference for High Performance Computing, Networking, Storage and Analysis, 2010, pp. 1–13.
- [21] D. OROZCO AND G. GAO, *Mapping the FDTD application to many-core chip architectures*, in Proceedings of the International Conference on Parallel Processing, Sept 2009, pp. 309–316.
- [22] D. OROZCO, E. GARCIA, AND G. GAO, *Locality optimization of stencil applications using data dependency graphs*, in Languages and Compilers for Parallel Computing, Springer Berlin Heidelberg, 2011, pp. 77–91.
- [23] S. SHRESTHA, J. MANZANO, A. MARQUEZ, J. FEO, AND G. R. GAO, *Jagged tiling for intratile parallelism and fine-grain multithreading*, in Proceedings of the 27th International Workshop on Languages and Compilers for Parallel Computing, Hillsboro, OR, USA, 2014.
- [24] H. STENGEL, J. TREIBIG, G. HAGER, AND G. WELLEIN, *Quantifying performance bottlenecks of stencil computations using the execution-cache-memory model*, (2014). In preparation.
- [25] R. STRZODKA, M. SHAHEEN, D. PAJAK, AND H.-P. SEIDEL, *Cache oblivious parallelograms in iterative stencil computations*, in Proceedings of the 24th ACM International Conference on Supercomputing, New York, NY, USA, 2010, ACM, pp. 49–59.
- [26] ———, *Cache accurate time skewing in iterative stencil computations*, in Proceedings of the International Conference on Parallel Processing, IEEE Computer Society, Sept. 2011, pp. 571–581.
- [27] Y. TANG, R. A. CHOWDHURY, B. C. KUSZMAUL, C.-K. LUK, AND C. E. LEISERSON, *The Pochoir stencil compiler*, in Proceedings of the Twenty-third Annual ACM Symposium on Parallelism in Algorithms and Architectures, New York, NY, USA, 2011, ACM, pp. 117–128.
- [28] D. UNAT, X. CAI, AND S. B. BADEN, *Mint: realizing CUDA performance in 3D stencil methods with annotated C*, in Proceedings of the international conference on Supercomputing, ACM, 2011, pp. 214–224.
- [29] G. WELLEIN, G. HAGER, T. ZEISER, M. WITTMANN, AND H. FEHSKE, *Efficient temporal blocking for stencil computations by multicore-aware wavefront parallelization*, in Computer Software and Applications Conference. 33rd Annual IEEE International, vol. 1, July 2009, pp. 579–586.
- [30] M. WITTMANN, G. HAGER, J. TREIBIG, AND G. WELLEIN, *Leveraging shared caches for parallel temporal blocking of stencil codes on multicore processors and clusters*, Parallel Processing Letters, 20 (2010), pp. 359–376.
- [31] D. G. WONNACOTT, *Using time skewing to eliminate idle time due to memory bandwidth and network limitations*, in International Parallel and Distributed Processing Symposium, 2000, pp. 171–180.
- [32] D. G. WONNACOTT AND M. M. STROUT, *On the Scalability of Loop Tiling Techniques*, in Proceedings of the 3rd International Workshop on Polyhedral Compilation Techniques, Berlin, 2013, pp. 3–11.
- [33] X. ZHOU, *Tiling optimizations for stencil computations*, PhD thesis, University of Illinois at Urbana-Champaign, 2013.